

DSRRTracker: Dynamic Search Region Refinement for Attention-based Siamese Multi-Object Tracking

JiaXu Wan¹, Hong Zhang¹, Jin Zhang², Yuan Ding¹, Yifan Yang³, Yan Li¹,
and Xuliang Li²

¹ School of Astronautics, Beihang University, Beijing, China

² School of Software, Beihang University, Beijing, China

³ School of Artificial Intelligence, Beihang University, Beijing, China

⁴

Abstract. Many multi-object tracking (MOT) methods follow the framework of “tracking by detection”, which associates the target objects-of-interest based on the detection results. However, due to the separate models for detection and association, the tracking results are not optimal. Moreover, the speed is limited by some cumbersome association methods to achieve high tracking performance. In this work, we propose an end-to-end MOT method, with a Gaussian filter-inspired dynamic search region refinement module to dynamically filter and refine the search region by considering both the template information from the past frames and the detection results from the current frame with little computational burden, and a lightweight attention-based tracking head to achieve the effective fine-grained instance association. Extensive experiments and ablation study on MOT17 and MOT20 datasets demonstrate that our method can achieve the state-of-the-art performance with reasonable speed.

Keywords: Multi-Object Tracking; Search region refinement; Attention-based tracking;

1 Introduction

Multi-object tracking (MOT) aims to estimate the trajectory of each individual object in a video sequence. The most typical approach to MOT is the “tracking-by-detection” [2,39,33,15,27,41,10,13,36,50], which first detects the objects-of-interest in the video and then the detected objects are used to guide the tracking process through some association methods (*e.g.*, IoU metric [2,36], deep neural networks [10,13], or Re-identification methods [39,32]). However, in the “tracking-by-detection” scheme, the data association is performed based on the detected objects from an independent off-the-shelf detector in separate stages. Thus, the potential synergistic information from the tracker and the detector are impossible to be jointly exploited in “tracking-by-detection”. Moreover, some

methods [1,19,13,10,20] use additional cumbersome association model independent of the detector to achieve high tracking performance, which however is hard to achieve the real-time tracking.

Some recent MOT methods [23,50,45,29,8] effectively borrow the idea of the association method used in single-object tracking (SOT) to improve the tracking results by either integrating the association module into the detector as a joint model or improving the association ability. However, when applying the SOT methods in the MOT tasks, it faces the issues of both computational burden (since each object in a scene require an individual tracker) and unsatisfied association, especially in the crowded scenes. The MOT methods generally deal with the computational issue by lightweight tracking heads [29] or limiting the search region for association [50]. For example, SiamMOT [29] uses a lightweight convolution tracking head to track instance without using the detection results. However, the SiamMOT fails to consider the available detection results provided by the detector and merely empirically set a search region. Differently, SOT-MOT [50] directly uses the detection results and reduces the search region of the future frames to the region defined by the detected bounding boxes. Though the search region is reduced, the detection and association are still performed in separate steps, limiting the final tracking performance.

In this paper, to deal with above issues, we propose an end-to-end SOT inspired joint tracking and detection MOT method, with a lightweight dynamic search region refinement module and a lightweight attention-based tracking head under the structure of a Siamese network.

Firstly, to extract synergistic features jointly from both the detector and the tracker, we take advantage of both the detection results of the current frame (*i.e.*, the detection prior) and the template information of the past frame (*i.e.*, the tracking prior) for association. To ensure the tracking speed, we design a Gaussian filter-inspired Dynamic search region refinement module to reduce the search region by filtering out the unrelated information within the region. Specifically, the search region in the current frame is dynamically adjusted based on a carefully designed Gaussian-inspired dynamic filter generator according to both the detection prior and the tracking prior, to filtering the noisy backgrounds and unrelated objects in a soft fashion to produce a more compact search region. Note that the idea of Gaussian-inspired filter generator used in our method are very different from the Gaussian filter used in traditional SOT. In SOT, the Gaussian filter is only used as a post-processing to obtain the final tracking results. We use it differently as a dynamic intermediate feature filter that contributes to the the followed tracking head networks, which helps learning more compact features for better association.

Secondly, based on the detection results of the past frame and the filtered search region of the current frame, we further propose a lightweight attention-based tracking head to achieve the effective association. The tracking head is a combination of self-attention and cross-attention modules. The self-attention modules aims at extracting more compact features from both the template and the coarse-grained filtered search region respectively to further reduce the back-

ground noise. The attended template and search region are fed into a cross-attention module to achieve the fine-grained instance association. Note that our attention-based tracker is designed to be lightweight with only one layer for each module and sharing backbone feature, which is different from the Transformer-based SOT methods [7,35] and MOT methods [31,9] with much smaller computational costs.

The contribution of this paper is three-fold: we propose an end-to-end multi-object tracking (MOT) method with (1) a lightweight Gaussian filter-inspired dynamic search region refinement module that adaptively filter the search region based on both detection and tracking priors, and (2) a lightweight attention-based tracking head for fine-grained feature enhancement and effective instance association. (3) Extensive experiments and analyses on MOT17 and MOT20 datasets in different settings validate the effectiveness of the proposed method.

2 Related Work

2.1 Multi-object tracking

Most multi-object tracking (MOT) methods [2,39,33,15,27,41,10,13,36,50] adopt the “tracking-by-detection” paradigm. These methods generally adopt a detector, such as FasterRCNN [25] or YOLO [24,4,12], to detect all objects in the video, and a separate Re-ID model [39] or deep neural networks [5] based tracker is then used to associate the objects. These impactful research advance the field of multi-object tracking. However, in the “tracking-by-detection” scheme, the data association is performed based on the detected objects from an independent off-the-shelf detector in separate stages. Thus, the potential synergistic information from the tracker and the detector are impossible to be jointly exploited in “tracking-by-detection”. Moreover, it is hard to achieve the real-time tracking with high performance due to the separate cumbersome models in the advanced deep learning methods.

Some recent MOT methods [23,50,45,29,8] effectively borrow the idea of the association method used in single-object tracking (SOT) to improve the tracking results by either integrating the association module into the detector as a joint model or improving the association ability. For example, SiamMOT[29], embeds the Siamese network tracking framework into Faster-RCNN[25] to achieve fast Siamese network-based multi-object tracking by light-weight tracking head and shared network parameters. Differently, SOTMOT[50] achieve the real-time tracking by limiting the search region of the tracker to the region covered merely by the detection results and using DCFST[49] to associate objects. However, these methods either ignore the detection prior or fully rely on it, which are both sub-optimal. Our work dynamically reduce the size of the search region by considering both the detection results of the current frame, as well as the template of the previous frame. Using the Dynamic Search Region Refinement Module, the network can dynamically adjust the search region in the current frame by filtering the features in a soft filter manner. In addition, our model

uses an attention-based tracking head to achieve the fine-grained instance association, which is different from most of the MOT methods.

2.2 Transformer-based Tracking

Recently, Transformer[34] has inspired many works for Single-object Tracking (SOT)[7,35], such as the well known TransT [7]. The attention-based modules in transformer structure can achieve better object association and achieves better results than the convolution-based Siamese network on the single-object tracking dataset. Some concurrent transformer-based MOT methods [31,44,9,47] are recently proposed. However, most of them adopt the cumbersome visual transformer models (*e.g.*, DETR[6]) as a blackbox model to obtain the final tracking results, without elaborately design of where and how to effectively take advantages of the self-attention and cross-attention layers. Moreover, due to the huge computation cost, it is hard for these methods to achieve real-time tracking. Differently, we enhance the localization of foreground objects within a box through self-attention and explicitly associate the template from the previous frame with the search region of the current frame through the cross-attention. Compared to the cumbersome TransTracker [31] and TransCenter [44], our lightweight attention-based tracking head can achieve much better results with only one-layer in each attention module.

3 Methodology

In this section, we describe the technical details of our model, which is named DSRTracker. As shown in Fig. 1, our model consists of a feature extraction backbone, a detection head (*e.g.*, YOLO[12]), a Dynamic Search Region Refinement Module, and an Attention-based Tracking Head.

Given an image pair of the past frame and the current frame, $\langle \mathbf{I}^t, \mathbf{I}^{t+\delta} \rangle$, and the tracking instances $R^t = \{\mathbf{r}_i^t\}_{i=1}^N$ from \mathbf{I}^t , our goal is to obtain the tracking instances $R^{t+\delta} = \{\mathbf{r}_j^{t+\delta}\}_{j=1}^M$ in $\mathbf{I}^{t+\delta}$. Each tracking instance $\mathbf{r}_i \in \mathbb{R}^5$ is a 5-dimensional vector that consists of the center location in x -axis, the center location in y -axis, the width, the height, and the object ID of the bounding box. We first define a set of search region instances $S^{t+\delta} = \{\mathbf{s}_i^{t+\delta}\}_{i=1}^N$ (with $\mathbf{s}_i \in \mathbb{R}^5$) in $\mathbf{I}^{t+\delta}$ based on the tracking instances R^t in \mathbf{I}^t . Then we extract features from the two frames with a shared feature extraction backbone, and the tracking instances and search regions in the feature map become $R_{\mathbf{F}}^t$ and $S_{\mathbf{F}}^{t+\delta}$, respectively. A region of interest align (ROIAlign) layer of Mask-RCNN[14] is then applied to all the instances in both $R_{\mathbf{F}}^t$ and $S_{\mathbf{F}}^{t+\delta}$ to obtain the corresponding features \mathbf{F}_R^t and $\mathbf{F}_S^{t+\delta}$. We also apply a detection head on the current frame features to obtain a set of detection instances in the feature map $D_{\mathbf{F}}^{t+\delta} = \{\mathbf{d}_k^{t+\delta}\}_{k=1}^K$ (with $\mathbf{d}_k \in \mathbb{R}^5$, where the ID is set as -1 since the detection results do not contain the ID information). The search region features $\mathbf{F}_S^{t+\delta}$ of $\mathbf{s}_i^{t+\delta}$ are then refined by a dynamic search region refinement module (DSRRM) based on the selected detection instances within the search region $D_{\mathbf{F},\mathbf{s}_i}^{t+\delta}$, the tracking instance $\mathbf{r}_{\mathbf{F},i}^t$,

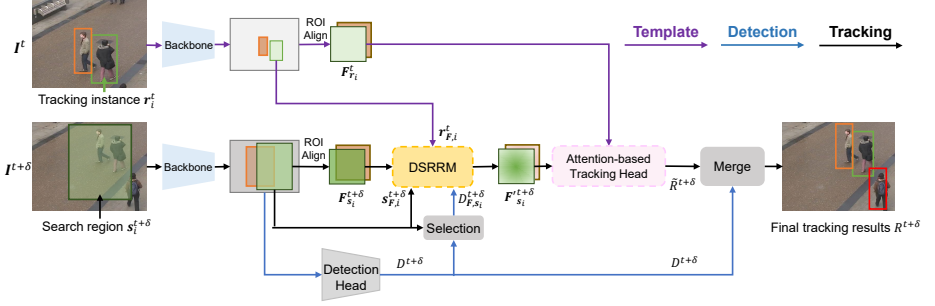


Fig. 1. Overview of our framework. Given frame I^t with tracking instance r_i^t and frame $I^{t+\delta}$, we first (1) define the search region $s_i^{t+\delta}$ in $I^{t+\delta}$ based on the tracking instance r_i^t in I^t and extract features from both r_i^t and $s_i^{t+\delta}$. (2) Then we detect the candidate objects $D^{t+\delta}$ in $I^{t+\delta}$. (3) Our proposed Dynamic Search Region Refinement Module (DSRRM) refine the features $F_{s_i}^{t+\delta}$ of the search region $s_i^{t+\delta}$ based on the detected instances $D_{F, s_i}^{t+\delta}$ selected within the search region and the tracking instance $r_{F, i}^t$ in the feature space. (4) An attention-based tracking head is proposed for object association between tracking instance features $F_{r_i}^t$ and the refined search region features $F_{s_i}^{t+\delta}$. (5) The final tracking results $R^{t+\delta}$ are obtained by merging the detection results $D^{t+\delta}$ with the tracking results $\tilde{R}^{t+\delta}$.

and the search region instance $s_{F, s_i}^{t+\delta}$. With the refined search region feature $F_{s_i}^{t+\delta}$ and the tracking instance feature $F_{r_i}^t$, an attention-based tracking head is applied for association. The final tracking results $R^{t+\delta}$ are obtained by merging the all the detection results $D^{t+\delta}$ with all the tracking results $\tilde{R}^{t+\delta}$.

3.1 Dynamic Search Region Refinement Module

In MOT, one of the key question is how to decide the proper size of the search region for efficient and effective object association. We argue that one-size may not fit all the cases. Hence, we propose a dynamic search region refinement module (DSRRM) as shown in Fig. 2 (a) using a Gaussian-inspired filter, with the adaptively generated scaling factor to dynamically adjust the search region by taking both the detection and tracking priors into account. The detection prior helps improving the precision of tracking, while the tracking prior compensates the cases of missed detections and keeps the object in track. Thus, the refinement module consists of a module to approximate the Detection and Tracking Prior Input, a Scaling Factor Generator, and a Dynamic Filter Generator.

The shaded module in light yellow of Fig. 2 (a) is the schematic process of this model. As shown in Fig. 2 (a), the input of the Scaling Factor Generator is the feature map $F_{s_i}^{t+\delta}$ extracted over the search region $s_i^{t+\delta}$ in frame $I^{t+\delta}$ with a detection and tracking prior mask $M_{s_i}^{t+\delta}$ generated through the set of detection results within the search region $D_{s_i}^{t+\delta}$ of frame $I^{t+\delta}$ and the tracking instances r_i^t of frame I^t . The output is a scaling factor α to characterize the detection confidence and the complexity of the scene. The dynamic filter generator then uses α to control the scale of the dynamic filter.

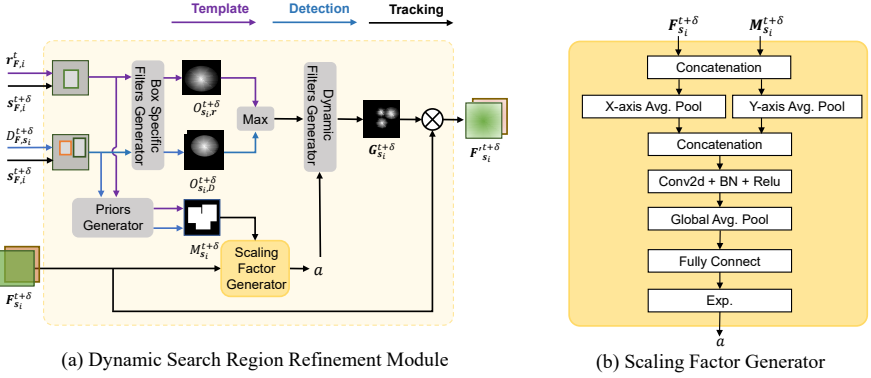


Fig. 2. (a) The details of our Dynamic Search Region Refinement Module (DSRRM). The module aims at refine the search region features $\mathbf{F}_{s_i}^{t+\delta}$ by a dynamic filter $\mathbf{G}_{s_i}^{t+\delta}$ obtained via the detected boxes $\mathbf{D}_{s_i}^{t+\delta}$ within the search region, the whole search region $\mathbf{s}_i^{t+\delta}$, and the tracking instance $\mathbf{r}_{F,i}^t$ of frame t . The filter $\mathbf{G}_{s_i}^{t+\delta}$ is dynamically adjusted by a scaling factor α predicted based on the features $\mathbf{F}_{s_i}^{t+\delta}$ as well as the detection and tracking priors $\mathbf{M}_{s_i}^{t+\delta}$. (b) The architecture of our Scaling Factor Generator.

Detection and Tracking Prior Generator. To effectively learn the scaling factor of the dynamic filter, we take the detection results of current frame (*i.e.*, the detection prior) as well as the tracking results of previous frame (*i.e.*, the tracking prior) into consideration. The joint detection and tracking priors are approximated by a binary input mask $\mathbf{M}_{s_i}^{t+\delta}$ in the search region, which is defined by the union of the detection results $\mathbf{D}_{s_i}^{t+\delta}$ and the tracking results \mathbf{r}_i^t . The prior is defined in such a way to not only guide the attention to the key foreground features but also implicitly reflect the crowdedness of a scene. Note the \mathbf{r}_i^t is also considered in $\mathbf{M}_{s_i}^{t+\delta}$ to avoid the trivial output of α due to the potential false negative of the detection results $\mathbf{D}_{s_i}^{t+\delta}$. Formally, the joint detection and tracking prior $\mathbf{M}_{s_i}^{t+\delta}$ is defined as follows,

$$\mathbf{M}_{s_i}^{t+\delta}(x, y) = \begin{cases} 1, & \text{if } (x, y) \text{ locates in } \mathbf{b}, \quad \forall \mathbf{b} \in \{\mathbf{D}_{F,s_i}^{t+\delta} \cup \mathbf{r}_{F,i}^t\} \\ 0, & \text{else} \end{cases} \quad (1)$$

where (x, y) is the coordinate of a specific point in the search region $\mathbf{s}_i^{t+\delta}$, $\{\mathbf{D}_{F,s_i}^{t+\delta} \cup \mathbf{r}_{F,i}^t\}$ is a set of detection or tracking instances, and $\mathbf{b} \in \mathbb{R}^5$ is an instance (with x_b, y_b, w_b, h_b, ID_b) belonging to the set. In other words, $\mathbf{M}_{s_i}^{t+\delta}(x, y)$ equal to 1 when the points (x, y) of the original image are located inside the detection bounding box of $\mathbf{b} \in \mathbf{D}_{F,s_i}^{t+\delta}$ or tracking bounding box of $\mathbf{r}_{F,i}^t$, otherwise it is 0. After getting the joint detection and tracking priors, the model channel-wisely concatenate $\mathbf{M}_{s_i}^{t+\delta}$ with the input feature map $\mathbf{F}_{s_i}^{t+\delta}$ to obtain the final prior input of the Scaling Factor Generator.

Scaling Factor Generator. By taking the detection and tracking prior into account, we design a network structure to adaptively learn the scaling factor α of the Gaussian-inspired dynamic filter. Intuitively, if the scene is very crowd,

the prior information should be emphasized to learn more discriminative features among different objects to avoid ID swap. We propose a neural network structure to learn the scaling factor α automatically based on the both the feature maps and the detection and tracking priors, as shown in Fig. 2 (b), which directly outputs a single α value. Formally:

$$\alpha = \mathcal{H}(\mathbf{F}_{\mathbf{s}_i}^{t+\delta}, M_{\mathbf{s}_i}^{t+\delta}; \Theta_{\mathcal{H}}) \quad (2)$$

where \mathcal{H} is the α generator network parameterized by $\Theta_{\mathcal{H}}$, $\mathbf{F}_{\mathbf{s}_i}^{t+\delta}$ is the feature map extracted over the search region $\mathbf{s}_i^{t+\delta}$ in frame $\mathbf{I}^{t+\delta}$, $M_{\mathbf{s}_i}^{t+\delta}$ is the rectangle mask generated by $\mathbf{r}_{\mathbf{F},i}^t$ and $D_{\mathbf{F},\mathbf{s}_i}^{t+\delta}$. The generator network \mathcal{H} takes the concatenation of $\mathbf{F}_{\mathbf{s}_i}^{t+\delta}$ and $M_{\mathbf{s}_i}^{t+\delta}$ as input. Then we pool the concatenated inputs from x-axis and y-axis respectively and then channel-wisely concatenate the pooled features to encode the spatial structure information of the features and the prior from different directions. A convolution layer with 1×1 kernels and a global average pooling are followed, which allows the interaction between the features and the prior. The final output is obtained by a fully connected layer with an exponential operation, which potentially both encodes the crowdness and characterizes different scenes.

Dynamic Filter Generator. The dynamic filter is generated based on the detection and tracking bounding boxes within the search region as well as the scaling factor α that dynamically takes the priors into account.

Inspired from the CenterNet[52], We propose the dynamic filter as,

$$G_{\mathbf{s}_i}^{t+\delta}(x, y) = e^{\frac{O_{\mathbf{s}_i}^{t+\delta}(x, y)}{\alpha^2}} \quad (3)$$

where $O_{\mathbf{s}_i}^{t+\delta}(x, y)$ is a box specific filter based on the closeness between the coordinates of each point (x, y) of the search region $\mathbf{s}_i^{t+\delta}$ and the center point $(x_{\mathbf{b}}, y_{\mathbf{b}})$ of each bounding box (*i.e.*, $\mathbf{b} \in \{D_{\mathbf{F},\mathbf{s}_i}^{t+\delta} \cup \mathbf{r}_{\mathbf{F},i}^t\}$) on the feature map.

For the point on each bounding box $\mathbf{b} \in \{D_{\mathbf{F},\mathbf{s}_i}^{t+\delta} \cup \mathbf{r}_{\mathbf{F},i}^t\}$, We define the filter $O_{\mathbf{s}_i,\mathbf{b}}^{t+\delta}(x, y)$ normalized by $w_{\mathbf{b}}^2 + h_{\mathbf{b}}^2$ as follows,

$$O_{\mathbf{s}_i,\mathbf{b}}^{t+\delta}(x, y) = -\frac{(x - x_{\mathbf{b}})^2 + (y - y_{\mathbf{b}})^2}{w_{\mathbf{b}}^2 + h_{\mathbf{b}}^2} \quad (4)$$

where $x_{\mathbf{b}}, y_{\mathbf{b}}, w_{\mathbf{b}}, h_{\mathbf{b}}$ represents the x-axis, the y-axis, the width, and the height of the center point of the bounding box \mathbf{b} on the feature map $\mathbf{F}_{\mathbf{s}_i}^{t+\delta}$, respectively. When all the distances are calculated, we take the maximum value for all feature maps to get the final filter $O_{\mathbf{s}_i}^{t+\delta}$.

$$O_{\mathbf{s}_i}^{t+\delta}(x, y) = \max_{\mathbf{b} \in \{D_{\mathbf{F}}^{t+\delta}, \mathbf{r}_{\mathbf{F},i}^t\}} \{O_{\mathbf{s}_i,\mathbf{b}}^{t+\delta}(x, y)\} \quad (5)$$

We choose to take the maximum values over the closeness defined by different box filters to keep the most significant values for better distinguishing different objects, which can especially benefit the crowd scenes.

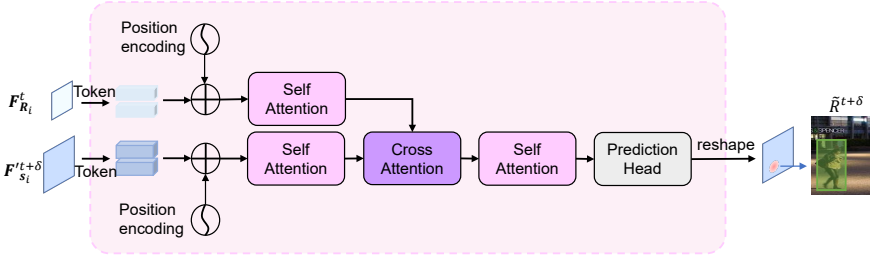


Fig. 3. The structure of our Attention-based Tracking Head.

After obtaining the dynamic filter, we apply the filter on the feature maps to highlight the the learned foreground features via element-wise multiplication as follows,

$$\mathbf{F}'_{s_i}{}^{t+\delta} = \mathbf{F}_{s_i}^{t+\delta} \odot \mathbf{G}_{s_i}^{t+\delta} \quad (6)$$

where $\mathbf{G}_{s_i}^{t+\delta}$ is obtained by broadcasting $G_{s_i}^{t+\delta}$ to have the same size as $\mathbf{F}_{s_i}^{t+\delta}$. The refined feature map $\mathbf{F}'_{s_i}{}^{t+\delta}$ is obtained by filtering the feature map $\mathbf{F}_{s_i}^{t+\delta}$ over the search region $s_i^{t+\delta}$ in frame $\mathbf{I}^{t+\delta}$ by the dynamic filter $G_{s_i}^{t+\delta}$ generated by our Dynamic Search Region Refinement Module.

3.2 Attention-based Tracking Head

We propose a lightweight attention-based tracking head to achieve the effective object association.

Attention-based Tracking Strategy. The structure of the module is shown in Fig. 3, which contains two 1-layer self-attention blocks and a 1-layer cross-attention block, followed by another 1-layer self-attention block. The module takes $\mathbf{F}_{R_i}^t$ and $\mathbf{F}'_{s_i}{}^{t+\delta}$ as inputs, which allows the model further attends to the foreground areas of the template and the filtered search region by the two self-attention blocks, respectively. The cross-attention module between the template and the filtered search region enables the message passing between them, and associates the correct target objects in the search region to the template. The final self-attention layer further refine the association results.

Prediction Head. To reduce the computational costs, we use a lightweight 3-layer fully connected (fc) layers to get the final predictions. In details, the dimension of the feature map $\mathbf{F}'_{s_i}{}^{t+\delta}$ is $H \times W \times C$, we feed the feature maps into the prediction head with three fc layers as: $\mathbf{F}'_{s_i}{}^{t+\delta} \rightarrow C \rightarrow C \rightarrow 7$, to get the final 7-dimensional predictions, representing the 2-dimensional foreground and background classification scores \mathbf{c}_i , the 4-dimensional bounding box size and location $\mathbf{p}(x, y)$, and the 1-dimensional central confidence[52] $w(x, y)$.

Loss. Given a triplet $(\mathbf{r}_{\mathbf{F},i}^t, \mathbf{s}_{\mathbf{F},i}^{t+\delta}, \mathbf{r}_{\mathbf{F},i}^{t+\delta})$, the tracking loss[29] of the tracking head is defined as follows:

$$\begin{aligned} \mathbf{L} = & \sum_{x,y} \ell_{\text{focal}}(\mathbf{c}_i(x,y), \mathbf{c}_i^*(x,y)) \\ & + \sum_{x,y} 1[\mathbf{c}_i^*(x,y) = 1] (w(x,y) \cdot \ell_{\text{reg}}(\mathbf{p}_i(x,y), \mathbf{p}_i^*(x,y))) \end{aligned} \quad (7)$$

where (x,y) enumerates all the valid locations in $\mathbf{s}_i^{t+\delta}$, $\mathbf{c}_i(x,y)$ is the classification scores, $\mathbf{p}_i(x,y)$ is the predicted bounding box, $w(x,y)$ is the centerness score, ℓ_{focal} is the focal loss for classification [17], and ℓ_{reg} is the GIOU Loss for regression [26]. Finally, \mathbf{c}_i^* and \mathbf{p}_i^* are the pixel-wise ground truth maps. $\mathbf{c}_i^*(x,y) = 1$ if (x,y) is within $\mathbf{r}_{\mathbf{F},i}^{t+\delta}$ and 0 otherwise. $\mathbf{p}_i^*(x,y) = [x - x_0^*, y - y_0^*, x_1^* - x, y_1^* - y]$ in which (x_0^*, y_0^*) and (x_1^*, y_1^*) correspond to the coordinates of the top-left and the bottom-right corner of ground truth bounding box $\mathbf{r}_{\mathbf{F},i}^{t+\delta}$. Similar to [53], we modulate ℓ_{reg} with $w(x,y)$, which is the centerness of location (x,y) w.r.t to the target instance $\mathbf{r}_{\mathbf{F},i}^{t+\delta}$ and is defined as $w(x,y) = \sqrt{\frac{\min(x-x_0, x_1-x)}{\max(x-x_0, x_1-x)} \cdot \frac{\min(y-y_0, y_1-y)}{\max(y-y_0, y_1-y)}}$.

Merge. We denote the set of predicted tracking instances on the feature map as $\hat{R}_{\mathbf{F}}^{t+\delta}$ from the tracking head, and convert the coordinates on the feature map to the coordinates on the original image to get the bounding box $\hat{R}^{t+\delta}$ on the original image. The final tacking results $R^{t+\delta}$ are obtained by merging the detection results $D^{t+\delta}$ with the tracking results $\hat{R}^{t+\delta}$. We use the standard spatial matching method for merging the results: the detected instances that spatially match (e.g., with $IoU \geq 0.5$) to any tracked instance are removed. Then, the standard *online* solver [1,51,3,40] is used to get $R^{t+\delta}$ by: 1) continuing the trajectory if its visibility confidence (v_i^t) is above the linking confidence γ ; 2) creating a trajectory if there is a non-matched detection and its confidence is above λ and 3) killing a trajectory if the visibility confidence (v_i^t) of the trajectory is below γ for consecutive τ frames.

4 Experiments

4.1 Implementation details

Network and Training Details. We use YOLOX[12] as our backbone network and detection head. For the hyperparameters, we set $r = 2$ by following SiamMOT[29], which indicates that the size of the search region is 2 times to the size of the tracking target \mathbf{r}_i^t . For our tracking head, the input feature maps are $\mathbf{F}_{\mathbf{r}_i}^t \in \mathbb{R}^{c \times 15 \times 15}$ and $\mathbf{F}_{\mathbf{s}_i}^{t+\delta} \in \mathbb{R}^{c \times 30 \times 30}$. Our tracking framework is pre-trained using *image training* on CrowdHuman[28] and is then trained on MOT17 using *video training* by following the previous MOT works [51,29]. The learning rate is set to 0.02 with 8 GPUs and the optimizer is the SGD with momentum. We train our model for 100K iterations and the batch size is set to 8 with 96 image regions per batch used to train the tracker.

Hyperparameters. The hyperparameters of the merge module for inference is the same as SiamMOT[29]. In the “public prediction” protocol, the linking confidence is $\gamma = 0.4$ and the detection confidence is $\lambda = 0.6$, and the model will keep a trajectory active until it is unseen for $\tau = 30$ frames.

Datasets. We evaluate our model on MOT17 and MOT20 datasets. MOT17[18] is a widely used multi-person tracking benchmark. It consists of 7 training and 7 test videos, ranging from 7 to 90 seconds long. The frame rate is between 14 and 30 fps, with and most of the videos are in size of 1920×1080 . MOT20[11] is a crowd multi-person tracking benchmark, which has much more crowded scenarios and occlusion cases. The average number of pedestrians in an image is 170 in the test set of MOT20.

Evaluation Metrics. We evaluate our method using both “public detection” and “private detection” protocols. The difference between the two protocols is that uses the provided detection results instead of results of our object detector in “public detection”, while the “private detection” means that we can freely select the object detector to provide the detection results. The private detector was trained using the training set of MOT17 and CrowdHuman by strictly following [51,29]. We report our results using several metrics under the standard evaluation protocol[18]: MOTA (Multiple Object Tracking Accuracy), IDF1 (ID F1 score), MT(Mostly tracked targets), ML(Mostly lost targets), FP (False Positives), FN (False Negatives), and IDsw (ID swap).

4.2 Results

We evaluate our model on MOT17 [18] under both the “private detection” protocol and “public detection” protocol, and MOT20 [11] datasets with the “private detection” protocol. We compare our method with other “tracking by detection” [31,36] [32,42,5,30,48,50] and “joint detection and tracking” [1,51,29,43,31,44,19,47] methods, including SOT-inspired methods[50,43,29], and Transformer-based methods[31] [44,47]. The results are shown in Tab. 1, 2, 3.

MOT17 Results. We report our results on the test set with the publicly released detection results and the private detection results, by strictly following the official MOT17 Challenge. Tab. 1 shows the comparisons of the public detection results on MOT17 dataset. From the results we can find that our method outperforms the state-of-the-art SOTMOT and SiamMOT method, with respect to both MOTA and IDF1 metrics.

Specifically, the tracking head in SiamMOT borrows the idea from SOT and associates the instances based on the template information. However, it fails to consider the detection results when available in MOT, leading to the unsatisfied results of IDF1. By contrast, SOTMOT fully relies on the detection results for object association, which is more sensitive to the capacity of the detector and achieves lower MOTA results. Differently, the dynamic search region refinement module in our DSRTracker takes both the detection results and template information into account and our attention-based tracking head further

Table 1. Results on MOT17 test set with public detection. The **Bold numbers** indicate that the method performs best, and the underlined numbers indicate that the method performs the second best, among the compared methods.

Method	MOTA↑	IDF1↑	MT↑	ML↓	FP↓	FN↓	IDsw↓
STRN [42]	50.9	56.5	20.1%	37.0%	27532	246924	2593
Tracktor++ [1]	53.5	52.3	19.5%	36.6%	12201	248047	2072
DeepMOT [43]	53.7	53.8	19.4%	36.6%	11731	247447	1947
Tracktor++ v2 [1]	56.5	55.1	21.1%	35.3%	<u>8866</u>	235449	3763
NeuralSolver [5]	58.8	61.7	28.8%	33.5%	17413	213594	1185
CenterTrack[51]	61.5	59.6	26.4%	31.9%	14076	200672	2583
TMOH[30]	62.1	62.0	-	-	10951	201195	<u>1897</u>
SOTMOT[50]	62.8	<u>65.9</u>	24.4%	33.0%	6556	201319	2017
SiamMOT[29]	<u>65.9</u>	63.3	<u>34.6%</u>	<u>23.9%</u>	18098	<u>170955</u>	3040
DSRRTracker(ours)	67.2	66.5	38.3%	20.5%	17875	164032	2896

improve the object features and achieve more accurate association. Thus, our method achieves the best and more balanced MOTA and IDF1 results.

In terms of private detection (Tab. 2), our method achieves the state-of-the-art IDF1 score and the second best MOTA result. Compared to SOTMOT[50], both the MOTA and IDF1 results are improved to a large margin by our method, which is benefited from our model making full use of better detection results and tracking results. Our method achieves lower MOTA results compared to CorrTracker[36] due to two main reasons. Firstly, CorrTracker uses information from multiple past frames and the current frame while we only rely on one previous frame together with the current frame. Secondly, the CorrTracker focuses more on how to improve the detection results, and thus their MOTA results are significantly improved, especially in the less crowd scenes such as MOT17. We argue that our method is orthogonal to CorrTracker, since we focus more on the design of the effective tracking head and our model can use any advanced detection methods as our detector.

We additionally compare our tracking head with the traditional tracking methods such as SORT[39] and JDE[38] with the same private detector (*i.e.*, Our Detector + SORT[39], and Our Detector + JDE[38]). The results show that our tracker outperforms the traditional tracking methods to a large margin, which further verifies that our joint detection and tracking method with our search region refinement module and the attention-based tracking head can effectively exploit the synergistic information from both the detector and tracker and improves the final results significantly.

MOT20 Results. As shown in Tab. 3, for the results of the MOT20 dataset with the private detection setting, our model outperforms all the compared baseline methods, which demonstrates that our method can effectively deal with more crowded scenarios in MOT20. Compared to CorrTracker, we notice a significant performance gain by our method in both MOTA and IDF1. Thus, our model can effectively overcome the false negative and imprecision of detection results in the

Table 2. Results on MOT17 test set with private detection. The **Bold numbers** indicate that the method performs best, and the underlined numbers indicate that the method performs the second best, among the compared methods.

Method	MOTA↑	IDF1↑	MT↑	ML↓	FP↓	FN↓	IDsw↓
DAN [32]	52.4	49.5	21.4%	30.7%	25423	234592	8431
TubeTK [19]	63.0	58.6	31.2%	19.9%	27060	177483	4137
MOTR [47]	65.1	66.4	33.0%	25.2%	45486	149307	2049
TransTracker [31]	65.8	56.9	32.2%	21.8%	24000	163683	5355
Chained-Tracker [21]	66.6	57.4	37.8%	18.5%	<u>22284</u>	160491	5529
CenterTrack [51]	67.8	64.7	34.6%	24.6%	18498	160332	3039
SOTMOT [50]	71.0	71.9	42.7%	<u>15.3%</u>	39537	118983	5184
TransCenter [44]	73.2	62.2	40.8%	18.5%	23112	123738	4614
FairMOT [48]	73.7	72.3	43.2%	17.3%	27507	117477	3303
CorrTracker [36]	76.5	<u>73.6</u>	<u>47.6%</u>	12.7%	29808	99510	3369
Our Detector + SORT[39]	66.7	65.2	33.1%	28.6%	22574	170432	5978
Our Detector + JDE[38]	70.6	70.9	40.1%	19.6%	28548	138374	3895
DSRRTracker (ours)	<u>75.6</u>	76.4	48.8%	16.2%	26983	<u>108186</u>	<u>2394</u>

Table 3. Results on MOT20 test set with private detection. The **Bold numbers** indicate that the method performs best, and the underlined numbers indicate that the method performs the second best, among the compared methods.

Method	MOTA↑	IDF1↑	MT↑	ML↓	FP↓	FN↓	IDsw↓
FairMOT [48]	61.8	67.3	68.8%	7.6%	103440	88901	5243
TransCenter [44]	61.9	50.4	49.4%	15.5%	<u>45895</u>	146347	4653
CorrTracker [36]	65.2	69.1	<u>66.4%</u>	<u>8.9%</u>	79429	<u>95855</u>	5183
CSTrack [16]	66.6	68.6	50.4%	15.5%	25404	144358	3196
RelationTrack [46]	67.2	70.5	62.2%	<u>8.9%</u>	61134	104597	4243
SOTMOT [50]	<u>68.6</u>	<u>71.4</u>	64.9%	9.7%	57064	101154	4209
DSRRTracker (ours)	70.4	71.9	65.1%	9.6%	48343	101034	<u>3739</u>

crowd scene by considering both detection results and template information (to improve MOTA), and can learn more discriminative object features by our dynamic filter and further achieve better association through the attention-based tracking head (to improve IDF1).

4.3 Ablation Study and Analysis

We report the results on the validation set for all the ablation studies in “public detection” protocol. We use “MOT17-05, MOT17-09, MOT17-13” of MOT17 as the validation set and other sequence as the training set.

Attention-based Tracking Head. We compare the convolution-based tracking head with our attention-based tracking head and the results are shown in Tab. 4. For fair comparison, we changed the backbone network in SiamMOT to the same YOLOX[12] backbone as we used and re-designed the original

Table 4. Ablation study of each module of our method on MOT17 validation set with public detection. FPS are calculated based on MOT17 videos with the origin image size and the platform is in Pytorch with 16GB V100. SiamMOT* indicates a variant of SiamMOT by using the same backbone network as our method and adding more parameters to the tracking head to have similar FLOPS as our method. We label our Cross-attention module, Self-attention modules, DSRRM module uses the detection prior only, DSRRM module uses the tracking prior only as CA, SA, Det., and Tra., respectively. MFLOPS is the computation of the tracking head.

Tracking Head		Det. Tra.	MOTA ↑	IDF1 ↑	FP ↓	FN ↓	IDsw ↓	FPS ↑	MFLOPS ↓
Conv-based	SiamMOT		62.3	61.8	5105	26222	603	23.0	92
	SiamMOT*		64.2	65.0	4535	25247	491	20.3	229
	SiamMOT*	✓ ✓	66.7	68.7	3942	23834	405	20.1	259
Attention-based	CA+SA		65.6	66.5	5521	23038	578	19.5	231
	2×SA+CA+SA		66.5	67.2	5486	22278	510	17.1	224
	2×SA+CA+SA	✓	62.9	61.4	4321	26615	456	17.1	268
	2×SA+CA+SA	✓ ✓	66.9	67.8	5220	23358	462	17.1	268
	2×SA+CA+SA	✓ ✓	68.6	69.1	4036	22181	398	17.1	268

convolution-based tracking head in SiamMOT to have the same FLOPS with our Attention-based tracking head by extending the number of channels from the original 64 to 256, which is named as SiamMOT*. By comparing line 2 and line 4,5 in Tab. 4, we can see that the performance improves significantly by replacing the convolution-based tracking head with our attention-based head, which validate the attention-based modules are more suitable for tracking tasks compared to convolution. Specifically, the results also show that by using cross attention module with the attention-based structure, the performance improves over the convolution-based structure. With the additional self-attention modules before the cross-attention module, the results are further improved. The results verify that the combination of the self-attention modules and the cross-attention module can well fit the tracking problem without additional computational costs. More visualization results can be found in the supplementary materials.

Dynamic Search Region Refinement Module. We also conduct more experiments to analyze the effectiveness of our dynamic search region refinement module (DSRRM), which are shown in the last three lines in Tab. 4. We analyze the results of the joint detection and tracking prior in details. “Det.” and “Tra.” indicate the variants of our “DSRRM” module with detection prior only and tracking prior only, respectively. The results show that merely relying on one of the priors is sub-optimal or even detrimental to the final results.

On one hand, for “Det.”, we can observe a decrease in FP and substantial increase in FN. The decrease in FP in “Det.” is because the tracking results is merely rely on the detection results. The significant increase in FN is due to the potential missed detections. Once there are missed detections, it is unlikely for the tracker to track it successfully in we only consider the detection prior.

On the other hand, when we only rely on the tracking prior as in “Tra.”, the performance is slightly improved, indicating that the tracking prior is essential or at least not detrimental to the tracking results. If we use both the detection

Table 5. Analysis of α in MOT17 validation set.

Model	MOTA \uparrow	IDF1 \uparrow	FP \downarrow	FN \downarrow	IDsw \downarrow
$\alpha = 1.0$	65.0	66.7	5078	23958	652
$\alpha = 2.0$	66.1	66.9	5532	22614	510
$\alpha = 3.0$	66.5	67.2	5486	22278	510
Dynamic α	68.6	69.1	4036	22181	398

and tracking priors, they jointly improve the final results. Thus, for the case of missed detection, the tracking prior can still keep the object in the track in many cases. While the detection prior helps improving the tracking precision. More visualization results of the DSRRM module can be found in the supplementary materials.

By comparing between line 2 and line 3 in Tab. 4, we can see that our DSRRM module is generic and can also improve the performance of the SiamMOT* tracking head by adding a DSRRM module in SiamMOT*.

In-depth analyses on α in our DSRRM. To evaluate the effectiveness of the proposed dynamic scaling factor α , we compare the results of using a constant α and our dynamic α in Tab. 5. We can find that the constant α does not work well compared to our dynamically learned α .

Furthermore, we evaluate how α in DSRRM is dynamically changed based on different scenes. Specifically, we roughly divide the MOT17 dataset into three subsets based on the object density of different sets[18] in MOT17 to characterize the crowdedness. We rename the three subsets as: *Sparse Set* (MOT17-05, MOT17-09, MOT17-11), *Medium Crowded Set* (MOT17-10, MOT17-13), and *Crowded Set* (MOT17-02, MOT17-04). The average values of α in the *Sparse Set*, *Medium Crowded Set*, and *Crowded Set* are 2.07, 1.83, and 1.61, respectively. As defined in Eq.(4), a large (*resp.*, small) α value corresponds to a large (*resp.*, small) variance of the dynamic filter, and thus the model rely less (*resp.*, more) on the detection and tracking prior. For the *Sparse Set* with less objects, the model can easily distinguish different objects in the less crowded scenes and thus the filter does not need to be compact, leading to larger average $\alpha = 2.07$ value for the better tracking results. In contrast, for the *Crowded Set*, the objects in a scene tend to be close to each other, and are even occluded by other objects. Thus the average $\alpha = 1.61$ and is learned to be small, such that the filter is more compact to alleviate the issue of ID swap between nearby objects in a crowded scene. For the *Medium Crowded Set*, the average $\alpha = 1.83$, which is between that of the *Crowded Set* and the *Sparse Set*. The results further verify that different scenes with various crowdedness require different α values to achieve good overall performance. More visualization results on the dynamic α can be found in the supplementary materials.

5 Conclusions

Observing the current “tracking by detection” MOT methods generally suffer from separate detection and association stages, which limits both the tracking performance and speed. We propose an end-to-end MOT method, based on a Gaussian filter-inspired dynamic search region refinement module to jointly take the template information and the detection results into consideration for association with little computational burden, and a lightweight attention-based tracking head to achieve the effective fine-grained instance association. The evaluations on MOT17 and MOT20 datasets demonstrate that our method can achieve the state-of-the-art performance with reasonable speed. For the limitations, our method only considers the tracking results from one previous frame to ensure the inference speed, and thus more temporal and correlation information from multiple previous frames are ignored. In the future, we will improve our method by using multiple frames without introducing much computational costs.

References

1. Bergmann, P., Meinhardt, T., Leal-Taixe, L.: Tracking without bells and whistles. In: ICCV. pp. 941–951 (2019) [2](#), [9](#), [10](#), [11](#), [24](#), [25](#)
2. Bewley, A., Ge, Z., Ott, L., Ramos, F., Upcroft, B.: Simple online and realtime tracking. In: 2016 IEEE International Conference on Image Processing (ICIP) (2016) [1](#), [3](#)
3. Bewley, A., Ge, Z., Ott, L., Ramos, F., Upcroft, B.: Simple online and realtime tracking. In: ICIP. pp. 3464–3468. IEEE (2016) [9](#)
4. Bochkovskiy, A., Wang, C.Y., Liao, H.Y.M.: Yolov4: Optimal speed and accuracy of object detection. arXiv preprint arXiv:2004.10934 (2020) [3](#)
5. Brasó, G., Leal-Taixé, L.: Learning a neural solver for multiple object tracking. In: Proceedings of the IEEE/CVF Conference on Computer Vision and Pattern Recognition. pp. 6247–6257 (2020) [3](#), [10](#), [11](#)
6. Carion, N., Massa, F., Synnaeve, G., Usunier, N., Kirillov, A., Zagoruyko, S.: End-to-end object detection with transformers. In: European Conference on Computer Vision. pp. 213–229. Springer (2020) [4](#)
7. Chen, X., Yan, B., Zhu, J., Wang, D., Yang, X., Lu, H.: Transformer tracking. In: Proceedings of the IEEE/CVF Conference on Computer Vision and Pattern Recognition (CVPR). pp. 8126–8135 (June 2021) [3](#), [4](#)
8. Chu, P., Ling, H.: Famnet: Joint learning of feature, affinity and multi-dimensional assignment for online multiple object tracking. In: Proceedings of the IEEE/CVF International Conference on Computer Vision (ICCV) (October 2019) [2](#), [3](#)
9. Chu, P., Wang, J., You, Q., Ling, H., Liu, Z.: Transmot: Spatial-temporal graph transformer for multiple object tracking. arXiv preprint arXiv:2104.00194 (2021) [3](#), [4](#)
10. Dai, P., Weng, R., Choi, W., Zhang, C., He, Z., Ding, W.: Learning a proposal classifier for multiple object tracking. In: Proceedings of the IEEE/CVF Conference on Computer Vision and Pattern Recognition (CVPR). pp. 2443–2452 (June 2021) [1](#), [2](#), [3](#)
11. Dendorfer, P., Rezatofighi, H., Milan, A., Shi, J., Cremers, D., Reid, I., Roth, S., Schindler, K., Leal-Taixé, L.: Mot20: A benchmark for multi object tracking in crowded scenes. arXiv preprint arXiv:2003.09003 (2020) [10](#)
12. Ge, Z., Liu, S., Wang, F., Li, Z., Sun, J.: Yolox: Exceeding yolo series in 2021. arXiv preprint arXiv:2107.08430 (2021) [3](#), [4](#), [9](#), [12](#)
13. Guo, S., Wang, J., Wang, X., Tao, D.: Online multiple object tracking with cross-task synergy. In: Proceedings of the IEEE/CVF Conference on Computer Vision and Pattern Recognition (CVPR). pp. 8136–8145 (June 2021) [1](#), [2](#), [3](#)
14. He, K., Gkioxari, G., Dollár, P., Girshick, R.: Mask r-cnn. In: ICCV. pp. 2961–2969 (2017) [4](#)
15. Henschel, R., Leal-Taixé, L., Cremers, D., Rosenhahn, B.: Fusion of head and full-body detectors for multi-object tracking. IEEE (2018) [1](#), [3](#)
16. Liang, C., Zhang, Z., Lu, Y., Zhou, X., Li, B., Ye, X., Zou, J.: Rethinking the competition between detection and reid in multi-object tracking. arXiv preprint arXiv:2010.12138 (2020) [12](#)
17. Lin, T.Y., Goyal, P., Girshick, R., He, K., Dollár, P.: Focal loss for dense object detection. In: ICCV. pp. 2980–2988 (2017) [9](#)
18. Milan, A., Leal-Taixé, L., Reid, I., Roth, S., Schindler, K.: Mot16: A benchmark for multi-object tracking. arXiv preprint arXiv:1603.00831 (2016) [10](#), [14](#), [20](#)

19. Pang, B., Li, Y., Zhang, Y., Li, M., Lu, C.: Tubetk: Adopting tubes to track multi-object in a one-step training model. In: Proceedings of the IEEE/CVF Conference on Computer Vision and Pattern Recognition. pp. 6308–6318 (2020) [2](#), [10](#), [12](#)
20. Peng, J., Wang, C., Wan, F., Wu, Y., Fu, Y.: Chained-tracker: Chaining paired attentive regression results for end-to-end joint multiple-object detection and tracking. The European Conference on Computer Vision (ECCV) (2020) [2](#)
21. Peng, J., Wang, C., Wan, F., Wu, Y., Wang, Y., Tai, Y., Wang, C., Li, J., Huang, F., Fu, Y.: Chained-tracker: Chaining paired attentive regression results for end-to-end joint multiple-object detection and tracking. In: European Conference on Computer Vision. pp. 145–161. Springer (2020) [12](#)
22. Peng, J., Wang, C., Wan, F., Wu, Y., Wang, Y., Tai, Y., Wang, C., Li, J., Huang, F., Fu, Y.: Chained-tracker: Chaining paired attentive regression results for end-to-end joint multiple-object detection and tracking. In: Proceedings of the European Conference on Computer Vision (2020) [24](#), [25](#)
23. Qi, C., Ouyang, W., Li, H., Wang, X., Yu, N.: Online multi-object tracking using cnn-based single object tracker with spatial-temporal attention mechanism. In: 2017 IEEE International Conference on Computer Vision (ICCV) (2017) [2](#), [3](#)
24. Redmon, J., Farhadi, A.: Yolov3: An incremental improvement. arXiv preprint arXiv:1804.02767 (2018) [3](#)
25. Ren, S., He, K., Girshick, R., Sun, J.: Faster r-cnn: Towards real-time object detection with region proposal networks. In: Advances in neural information processing systems. pp. 91–99 (2015) [3](#)
26. Rezaatoughi, H., Tsai, N., Gwak, J., Sadeghian, A., Reid, I., Savarese, S.: Generalized intersection over union: A metric and a loss for bounding box regression. In: Proceedings of the IEEE/CVF Conference on Computer Vision and Pattern Recognition. pp. 658–666 (2019) [9](#)
27. Ristani, E., Tomasi, C.: Features for multi-target multi-camera tracking and re-identification. In: Proceedings of the IEEE Conference on Computer Vision and Pattern Recognition (CVPR) (June 2018) [1](#), [3](#)
28. Shao, S., Zhao, Z., Li, B., Xiao, T., Yu, G., Zhang, X., Sun, J.: Crowddhuman: A benchmark for detecting human in a crowd. arXiv preprint arXiv:1805.00123 (2018) [9](#)
29. Shuai, B., Berneshawi, A., Li, X., Modolo, D., Tighe, J.: Siammot: Siamese multi-object tracking. In: Proceedings of the IEEE/CVF Conference on Computer Vision and Pattern Recognition (CVPR). pp. 12372–12382 (June 2021) [2](#), [3](#), [9](#), [10](#), [11](#), [22](#)
30. Stadler, D., Beyerer, J.: Improving multiple pedestrian tracking by track management and occlusion handling. In: Proceedings of the IEEE/CVF Conference on Computer Vision and Pattern Recognition. pp. 10958–10967 (2021) [10](#), [11](#)
31. Sun, P., Jiang, Y., Zhang, R., Xie, E., Cao, J., Hu, X., Kong, T., Yuan, Z., Wang, C., Luo, P.: Transtrack: Multiple-object tracking with transformer. arXiv preprint arXiv:2012.15460 (2020) [3](#), [4](#), [10](#), [12](#)
32. Sun, S., Akhtar, N., Song, H., Mian, A.S., Shah, M.: Deep affinity network for multiple object tracking. IEEE transactions on pattern analysis and machine intelligence (2019) [1](#), [10](#), [12](#)
33. Tang, S., Andriluka, M., Andres, B., Schiele, B.: Multiple people tracking by lifted multicut and person re-identification. In: Proceedings of the IEEE Conference on Computer Vision and Pattern Recognition. pp. 3539–3548 (2017) [1](#), [3](#)
34. Vaswani, A., Shazeer, N., Parmar, N., Uszkoreit, J., Jones, L., Gomez, A.N., Kaiser, L., Polosukhin, I.: Attention is all you need. In: Advances in neural information processing systems. pp. 5998–6008 (2017) [4](#)

35. Wang, N., Zhou, W., Wang, J., Li, H.: Transformer meets tracker: Exploiting temporal context for robust visual tracking. In: Proceedings of the IEEE/CVF Conference on Computer Vision and Pattern Recognition (CVPR). pp. 1571–1580 (June 2021) [3](#), [4](#)
36. Wang, Q., Zheng, Y., Pan, P., Xu, Y.: Multiple object tracking with correlation learning. In: Proceedings of the IEEE/CVF Conference on Computer Vision and Pattern Recognition. pp. 3876–3886 (2021) [1](#), [3](#), [10](#), [11](#), [12](#), [24](#), [25](#)
37. Wang, Y., Kitani, K., Weng, X.: Joint object detection and multi-object tracking with graph neural networks. In: 2021 IEEE International Conference on Robotics and Automation (ICRA). pp. 13708–13715 (2021). <https://doi.org/10.1109/ICRA48506.2021.9561110> [24](#), [25](#)
38. Wang, Z., Zheng, L., Liu, Y., Wang, S.: Towards real-time multi-object tracking. The European Conference on Computer Vision (ECCV) (2020) [11](#), [12](#)
39. Wojke, N., Bewley, A., Paulus, D.: Simple online and realtime tracking with a deep association metric. IEEE pp. 3645–3649 (2017) [1](#), [3](#), [11](#), [12](#)
40. Wojke, N., Bewley, A., Paulus, D.: Simple online and realtime tracking with a deep association metric. In: 2017 IEEE international conference on image processing (ICIP). pp. 3645–3649. IEEE (2017) [9](#)
41. Xu, H., Jiang, C., Liang, X., Li, Z.: Spatial-aware graph relation network for large-scale object detection. In: Proceedings of the IEEE/CVF Conference on Computer Vision and Pattern Recognition (CVPR) (June 2019) [1](#), [3](#)
42. Xu, J., Cao, Y., Zhang, Z., Hu, H.: Spatial-temporal relation networks for multi-object tracking. In: Proceedings of the IEEE/CVF International Conference on Computer Vision. pp. 3988–3998 (2019) [10](#), [11](#)
43. Xu, Y., Ban, Y., Alameda-Pineda, X., Horaud, R.: Deepmot: a differentiable framework for training multiple object trackers. arXiv preprint arXiv:1906.06618 (2019) [10](#), [11](#)
44. Xu, Y., Ban, Y., Delorme, G., Gan, C., Rus, D., Alameda-Pineda, X.: Transcenter: Transformers with dense queries for multiple-object tracking. arXiv preprint arXiv:2103.15145 (2021) [4](#), [10](#), [12](#)
45. Yin, J., Wang, W., Meng, Q., Yang, R., Shen, J.: A unified object motion and affinity model for online multi-object tracking. IEEE (2020) [2](#), [3](#)
46. Yu, E., Li, Z., Han, S., Wang, H.: Relationtrack: Relation-aware multiple object tracking with decoupled representation. arXiv preprint arXiv:2105.04322 (2021) [12](#)
47. Zeng, F., Dong, B., Wang, T., Chen, C., Zhang, X., Wei, Y.: Motr: End-to-end multiple-object tracking with transformer. arXiv preprint arXiv:2105.03247 (2021) [4](#), [10](#), [12](#)
48. Zhang, Y., Wang, C., Wang, X., Zeng, W., Liu, W.: Fairmot: On the fairness of detection and re-identification in multiple object tracking. arXiv preprint arXiv:2004.01888 (2020) [10](#), [12](#), [24](#), [25](#)
49. Zheng, L., Tang, M., Chen, Y., Wang, J., Lu, H.: Learning feature embeddings for discriminant model based tracking-supplementary material. In: ECCV (2020) [3](#)
50. Zheng, L., Tang, M., Chen, Y., Zhu, G., Wang, J., Lu, H.: Improving multiple object tracking with single object tracking. In: Proceedings of the IEEE/CVF Conference on Computer Vision and Pattern Recognition. pp. 2453–2462 (2021) [1](#), [2](#), [3](#), [10](#), [11](#), [12](#), [24](#), [25](#)
51. Zhou, X., Koltun, V., Krähenbühl, P.: Tracking objects as points. In: European Conference on Computer Vision. pp. 474–490. Springer (2020) [9](#), [10](#), [11](#), [12](#), [24](#), [25](#)
52. Zhou, X., Wang, D., Krähenbühl, P.: Objects as points. arXiv preprint arXiv:1904.07850 (2019) [7](#), [8](#)

53. Zhu, C., Chen, F., Shen, Z., Savvides, M.: Soft anchor-point object detection. In: Computer Vision–ECCV 2020: 16th European Conference, Glasgow, UK, August 23–28, 2020, Proceedings, Part IX 16. pp. 91–107. Springer (2020) [9](#)

A In-depth analyses on α in our DSRRM.

To further conduct more in-depth analyses on the learned α in our dynamic search region refinement module (DSRRM), we roughly divide the MOT17 dataset into three subsets of different sets[18] in MOT17 based on the number of objects in a scene to characterize the crowdedness. We rename the three subsets as: *Sparse Set* (MOT17-05, MOT17-09, MOT17-11), *Medium Crowded Set* (MOT17-10, MOT17-13), and *Crowded Set* (MOT17-02, MOT17-04). As shown in Figure S1, the *Sparse Set* contains the scenes with less number of objects, the *Medium Crowded Set* contains more objects than that of *Sparse Set*, and the *Crowded Set* consists of the most crowded scenes.

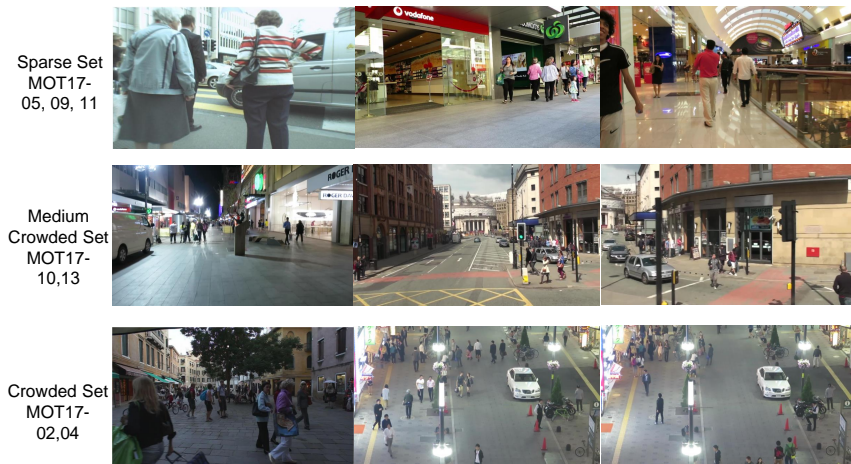


Fig. S1. The example scenes in different subsets of the MOT17 (e.g., *Sparse Set* (MOT17-05, MOT17-09, MOT17-11), *Medium Crowded Set* (MOT17-10, MOT17-13), *Crowded Set* (MOT17-02, MOT17-04)).

We approximate the shape of the distribution of α on the the three subsets, by recording the number of samples that produces different α values (forming a histogram of α) after optimization. The histograms are shown in Figure S2. The horizontal axis indicates different α values, while the vertical axis represents the number of instances that produce the corresponding α values. The curves in different colors indicate the histograms of the each subset (e.g., *Sparse Set* (MOT17-05, MOT17-09, MOT17-11) in green, *Medium Crowded Set* (MOT17-10, MOT17-13) in orange, and *Crowded Set* (MOT17-02, MOT17-04) in blue), as well as the overall MOT-17 dataset (in red).

The results demonstrate that the histograms of α vary on different subsets. As defined in Eq.(3) of the main paper, a large (*resp.*, small) α value corresponds

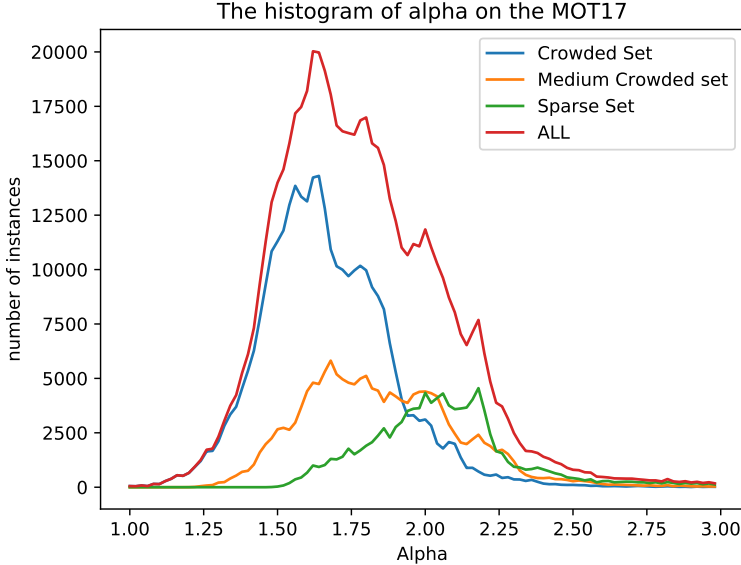


Fig. S2. The histogram of α on 3 subsets and all sets of MOT17 (*Sparse Set* includes MOT17-05, MOT17-09 and MOT17-11, *Medium Crowded Set* includes MOT17-10 and MOT17-13, *Crowded Set* includes MOT17-02 and MOT17-04))

to a large (*resp.*, small) variance of the dynamic filter, and thus the model rely less (*resp.*, more) on the detection and tracking prior. For the *Crowded Set*, the objects in a scene are tend to be close to each other, and even occluded by other objects. Thus, the blue curve in Figure S2 demonstrates that the α values are learned to be small, such that the filter is more compact to alleviate the issue of ID swap between nearby objects in a crowded scene. In contrast, for the *Sparse Set* with less objects, the model can easily distinguish different objects in the less crowded scenes and thus the filter does not need to be compact, leading to larger α values (the green curve) for the better tracking results. For the *Medium Crowded Set*, the α values are also concentrated on a medium value as shown in the orange curve.

B Structures of different variants of the tracking head.

In the Table(4) of the main paper, we compare the baseline convolution-based tracking head (*i.e.*, SiamMOT), a variation structure of the attention-based tracking head (*i.e.*, CA+SA), and our final tracking head (*i.e.*, $2 \times \text{SA} + \text{CA} + \text{SA}$). Figure S3 illustrates and compares the details of the three structures. In details, Figure S3 (a) is the structure of SiamMOT and SiamMOT*. SiamMOT* indicates a variant of SiamMOT by using the same backbone network as our method and adding more parameters to the tracking head to the have similar FLOPS as

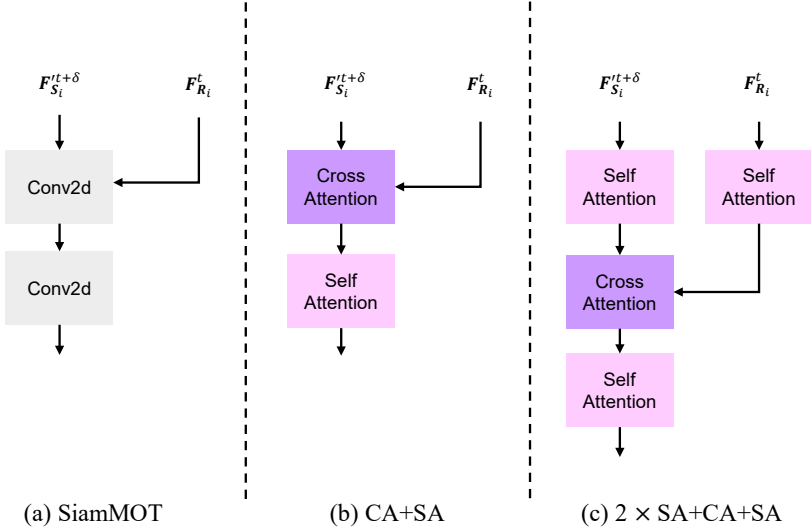


Fig. S3. Different variants of the tracking head structures for ablation study. (a) the convolution-based SiamMOT [29] tracking head, (b) the CA+SA tracking head, (c) our final 2× SA+CA+SA tracking head.

our method. Figure S3 (b) is the structure of SA+CA and Figure S3 (c) is the structure of 2×SA+CA+SA.

Our final Attention-based Tracking Head (ATH) (with 2×SA+CA+SA structure) first uses two self-attention blocks to process the input template features $F_{r_i}^t$ and the refined search region features $F_{s_i}^{t+\delta}$, respectively, which allows the model further attends to the foreground areas of the template and the refined search region. The followed cross-attention module enables the message passing between the template and the search region, and associates the correct target objects in the search region to the template. The final self-attention layer further refine the association results.

C Qualitative Results.

We qualitatively visualize the learned dynamic filter, as well as the attention maps learned by the attention-based tracking head in Figure S4.

The “(1) Input Image” line indicates the original input frames in a video sequence. The “(2) Dynamic Filter (DFs)” line demonstrates the dynamically learned filters by our DSRRM module. It can be seen that the variance of the filters are different. Specifically, in the crowd scene with multiple nearby persons, the variance of the filter is automatically learned to be small to alleviate ID swap. In the scene with a single object, the model can easily distinguish the object with its surrounding background, and thus the variance of the filter is large since the filter does not need to be learned to be compact.

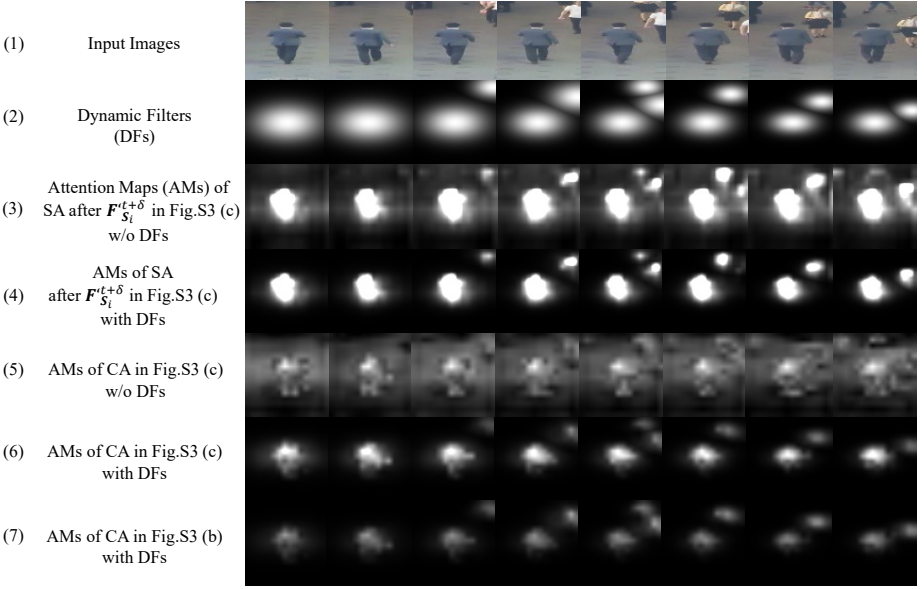


Fig. S4. Visualization of the dynamic filter and the attention maps of different variants of our method. From top to bottom are, (1) the original image, (2) the DSRRM-generated Dynamic filters (DFs), (3) Attention Maps (AMs) of SA after $F'_{s_i}{}^{t+\delta}$ in Figure S3 (c) w/o Dynamic filters, (4) Attention Maps of SA after $F'_{s_i}{}^{t+\delta}$ in Figure S3 (c) with Dynamic filters, (5) Attention Maps of CA in Figure S3 (c) w/o Dynamic filters, (6) Attention Maps of CA in Figure S3 (c) with Dynamic filters, (7) Attention Maps of CA in Figure S3 (b) with Dynamic filters.

The “(3) Attention Maps (AMs) of SA after $F'_{s_i}{}^{t+\delta}$ in Figure S3 (c) w/o DFs” with “(4) AMs of SA after $F'_{s_i}{}^{t+\delta}$ in Figure S3 (c) with DFs” are the two variants of the attention maps of the self-attention module of our final tracking head with the dynamic filter or not, respectively. We can observe that many noisy backgrounds and unrelated objects are highlighted when using the self-attention alone without the dynamic filter. By contrast, with the dynamic filter, the attention map of the self-attention module can well filter out more unrelated backgrounds and objects.

Similarly, the “(5) AMs of CA in Figure S3 (c) w/o DFs” and “(6) AMs of CA in Figure S3 (c) with DFs” are the attention maps of the cross-attention module of our final tracking head, with the dynamic filter or not, respectively. It can be seen that without the dynamic filter, the detrimental effects of the noisy backgrounds and unrelated objects are enlarged in the cross-attention layer.

The last row of the “(7) AMs of CA in Figure S3 (b) with DFs” means the attention map of the cross-attention module with only the dynamic filter when removing the first two self-attention modules in the tracking head. Compared with “(6) AMs of CA in Figure S3 (c) with DFs”, the object-of-interest is not

well highlighted and the surrounding noises are not well suppressed in “(7) AMs of CA in Figure S3 (b) with DFs”.

In summary, based on the visualizations and comparisons, our observations are three-fold. **Firstly**, for our dynamic search region refinement module (DSRRM), it can be seen that the learned filters can dynamically filter different scenes. For example, in the crowded scenes, the model is more prone to ID swap, and thus the tracking head tends to rely on the detection results to learn more discriminative object features and reduce the search region for each object to distinguish different objects better. **Secondly**, for our attention-based tracking head, the self-attention modules and the cross-attention module jointly achieve good tracking results. Specifically, the self-attention module help the model attend to the foreground position of the target obejects, while the cross-attention module can achieve fine-grained association of the target objects between different frames. **Thirdly**, we can also verify that the DSRRM module and the self-attention modules in our attention-based tracking head synergistically improve the tracking results from different perspectives. The DSRRM module tries to filter the search region globally and roughly based on the crowedness of the scene or the hardness of the detection task. While the self-attention modules in our attention-based tracking head further locally and finely refine each individual object.

D Speed analysis.

We report the speed-wise comparison results between our method with both “tracking by detection” baseline methods[36,48,37,50,22] and “joint detection and tracking” baseline methods[51,1]. Table S1 shows the results on MOT17 and MOT20 test set with “private detection” protocol on the platform with single 16GB V100 GPU and Pytorch environment.

We can find that on both the MOT17 and MOT20 datasets, our method mostly achieves the state-of-the-art or comparable and more balanced MOTA and IDF1 results and the second best speed-wise metric (*i.e.*, FPS) compared to all 7 recent baseline methods. Note that though our speed-wise performance is lower than FairMOTv2, our MOTA and IDF1 results are significantly better.

Table S1. Speed analysis on test set of MOT17 and MOT20 with private detection. The **Bold numbers** indicate that the method performs best, and the underlined numbers indicate that the method performs the second best, among the compared methods.

Method	MOT17			MOT20		
	MOTA \uparrow	IDF1 \uparrow	FPS \uparrow	MOTA \uparrow	IDF1 \uparrow	FPS \uparrow
CorrTracker[36]	76.5	<u>74.3</u>	14.8	65.2	69.1	8.5
FairMOTv2[48]	73.7	72.3	25.4	66.6	68.2	13.2
GSTD[37]	73.2	66.5	2.3	67.1	67.5	0.9
SOTMOT[50]	71.0	71.9	16.0	<u>68.6</u>	<u>71.4</u>	8.5
CenterTracker[51]	67.8	64.7	3.8	/	/	/
CTracker[22]	66.6	57.4	6.8	/	/	/
Tracker++v2[1]	56.2	54.9	1.8	/	/	/
DSRRTracker(ours)	<u>75.6</u>	76.4	<u>17.3</u>	70.4	71.9	<u>10.1</u>